Journal of Computer-Aided Molecular Design, **12:** 351–360, 1998.
KLUWER/ESCOM

Modelling a 3D structure for EgDf1 from *Echinococcus granulosus*: putative epitopes, phosphorylation motifs and ligand

M. Paulino, A. Esteves[a], M. Vega, G. Tabares, R. Ehrlich[a] & O. Tapia[b,*]
Department of Quantum Chemistry, Faculty of Chemistry. Universidad de la República, Uruguay; [a]*Institute of Biology. Faculty of Sciences. Universidad de la República. Uruguay;* [b]*Department of Physical Chemistry, Uppsala University, Box 532, 75121 Uppsala, Sweden*

Received 20 October 1997; Accepted 10 December 1997

Key words: Echinococcus granulosus, EgDf1, epitopes, modelling, phosphorylation sites

Summary

EgDf1 is a developmentally regulated protein from the parasite *Echinococcus granulosus* related to a family of hydrophobic ligand binding proteins. This protein could play a crucial role during the parasite life cycle development since this organism is unable to synthetize most of their own lipids de novo. Furthermore, it has been shown that two related protein from other parasitic platyhelminths (Fh15 from *Fasciola hepatica* and Sm14 from *Schistosoma mansoni*) are able to confer protective inmunity against experimental infection in animal models. A three-dimensional structure would help establishing structure/function relationships on a knowledge based manner.

3D structures for EgDf1 protein were modelled by using myelin P2 (mP2) and intestine fatty acid binding protein (I-FABP) as templates. Molecular dynamics techniques were used to validate the models. Template mP2 yielded the best 3D structure for EgDf1. Palmitic and oleic acids were docked inside EgDf1.

The present theoretical results suggest definite location in the secondary structure of the epitopic regions, consensus phosphorylation motifs and oleic acid as a good ligand candidate to EgDf1. This protein might well be involved in the process of supplying hydrophobic metabolites for membrane biosynthesis and for signaling pathways.

Introduction

EgDf1 is a protein identified by differential inmunoscreening from a λgt11 cDNA library of protoscoleces of *Echinococcus granulosus* [1–6], the causative agent of hidatid disease, which is a major zoonosis all over the world. The molecular and cellular bases of *E. granulosus* development are still largely unknown. Nevertheless, recent progress in developmental biology, showing common regulatory processes between distant organisms, and the increasing knowledge concerning the development of other platyhelminths, are providing important clues for studying the molecular basis of *E. granulosus* development.

EgDf1 has a molecular weight of ca. 15 kDa and belongs to a multigenic family of structurally related low molecular weight cytosolic proteins which includes fatty acid binding proteins (FABPs), cellular retinoid transporter proteins (cRtPs), and mP2 (myelin P2 protein). Several vertebrate and invertebrate proteins of the group have been structurally characterized, including: FABPs from intestine (I-FABP), heart muscle (H-FABP), adipose tissue (aP2), mP2, mammary gland derived inhibitor protein (MDGI) [7–9], gastrortropin, a FABP from *L. migratoria* and from *Manduca sexta* [10]. The differences in structure, ligand-binding properties and tissue distribution of the different members in the family suggest tissue-specific structure specialization of this diverse group of proteins. The 3D structure of EgDf1 has not yet been experimentally determined, but there are good reasons to believe that it will show the characteristic topology of this family. This is the basic hypothesis on which this work rest.

*To whom correspondence should be addressed.

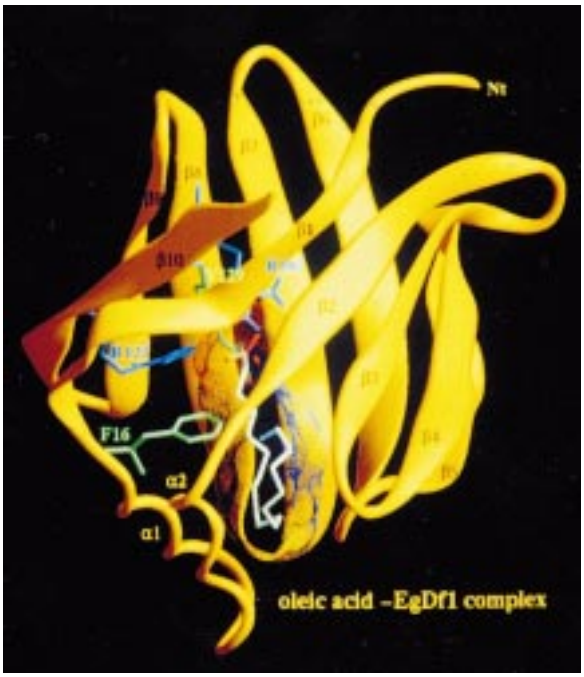

Figure 1. Ribbons model [47] of the backbone structure of EgDf1 modelled from mP2. Oleic acid model (white sticks) and its van der Waals surface (dot surface) docked to the binding site of the protein is shown.

In this paper, a 3D structure for EgDf1 is constructed by using the intracellular hydrophobic ligand-binding proteins whose members have structures determined with X-ray diffraction methods to high resolution. Prediction of three-dimensional structures using computer-aided techniques is becoming a widespread and fairly reliable approach [11–14]. Here, molecular graphics and molecular dynamics techniques are used to check upon the stability towards thermal fluctuations of the energy minimized structure. The structure derived from mP2 turns out to be the most reliable. From the topologic features of the putative structure, oleic acid is suggested to be one of the possible substrates of EgDf1. The hydrophilic region 9–14 (Lys-Met-Glu-Lys-Ser-Glu) is identified as a possible epitope following the experimental results by Esteves et al. [1, 2]. Consensus phosphorylation sites already identified with different methods [2] are shown here to be structurally accessible. Figure 1 pictorially summarizes these results.

Materials and methods

Templates

Hydrophobic ligand binding proteins with β-barrel topology. The transport of small hydrofobic molecules has been solved in intracellular and extracellular media through proteins with similar barrel topology. The extracellular hydrophobic ligand-binding protein family, also known as lipocalins, includes, among others, retinol binding protein (RBP), microglobulin, β-lactoglobulin and bilin-binding protein. The member of this family share low sequence homology and are involved in the transport of small hydrophobic ligands. The intracellular hydrophobic ligand-binding protein family is defined by small intracellullar proteins that bind ligands such as fatty acids, eikosanoids and retinoids. It includes FABPs, cRtPs, and myelin P2 protein.

Extracellular hydrophobic ligand-binding proteins. This family folds as a β-barrel over which stacks a four turn α-helix. Eight antiparallel strands wrap around the barrel so that part of the first is flanked by the last strand. This results in two orthogonal β-sheets where the first strand is shared by them with two possible entrance/exit channels.

In the serum RBP, the retinol molecule sits in the center of this barrel with the β-ionone ring innermost. At the entrance, which is formed by residues from three loops, the alcohol group of the ligand is slightly exposed to solvent [15, 16].

In myelin P2, crystallographic studies [17] detected the carboxyl group of the bound fatty acid placed between the guanidinium groups of the arginines Arg106 and Arg126 and close to the hydroxyl group of tyrosine Tyr128 in the binding pocket. The remainder of the binding pocket is made up of residues Val115, Ile104, Tyr19, Asp76, Phe16 and Met20.

Modelling approach

Molecular graphics and computer-assisted simulations are useful tools in constructing 3D structures of homologous proteins and designing biomolecules with appropriate ligands [12–14, 19–25]. Moreover, molecular dynamics (MD) simulations offer practical ways to validate static modelled structures [26]. As by-products, one obtains averaged geometric structures and atomic fluctuation patterns. These latter may help identify plastic zones in the structure.

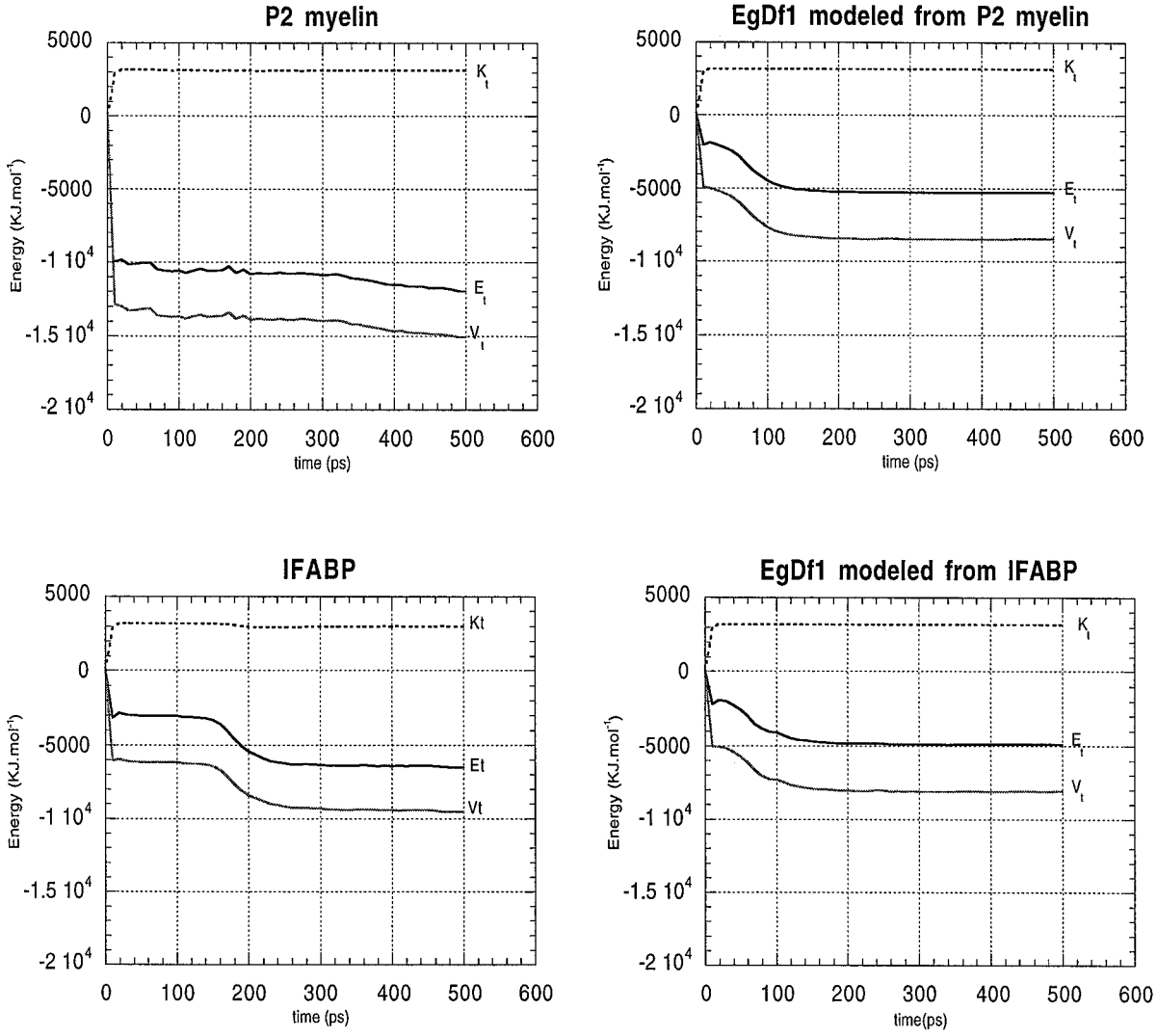

Figure 2. Time evolution of the potential, total and kinetic energies of crystallografic mP2 and I-FABP structures and EgDf1 modelled from IFABP and from mP2

Previous modelling work. Model building techniques have been used to predict the structure of a molecular complex between RBP and its carrier protein transthyretin (TTR). This followed the theoretical prediction of apo-fold stability [18]. In the plasma cells, a complex is formed between holo-RBP and the thyroxine-binding TTR tetramer. This complex is then recognized by a cell surface receptor, which delivers the vitamin to the cell. Since RBP probably interacts with more than one intracellular protein when receiving the retinol in the liver hepatocytes, the molecule is involved in at least four different interaction types. The model complex provides a molecular basis to describe the experimental results [19]. Later on, a crystal structure of a hexameric complex $(RBP)_2$-TTR was reported by Monaco et al. [20]. This permitted an evaluation of the model structure which was constructed under the commonly accepted view of a $(RBP)_4$-TTR complex. As noted by Monaco et al., while the model explained a number of experimental issues, and although some of the residues involved in the contact were correctly identified, the theoretical model was different from the X-ray structure. A close look at the real structure and the positioning of RBP in the model (built up with no previous structural clues) clearly

shows the quality of the model. Its structure was not that far from the real one.

Modelling EgDf1. EgDf1 modelling was carried out by a molecular replacement method. The overlapping of the primary sequences of the homologous proteins mP2 and I-FABP was obtained from the EMBL-Heidelberg Genbank. Homology percentages were obtained taking as conservative replacements those of residues with similar polarity or electrostatic charges. Following this criterion, EgDf1 has 62.6% homology and 44.3% identity with respect to myelin P2 and 51.1% homology 30.5% identity with respect to I-FABP. The replacement of non 3D conserved side chains was carried out with the TOM/mdFRODO [27, 28] program as follows: (a) replacement from amino acids 1 to 57 and refinement of this segment (1000 steps); (b) insertion after amino acid 58; (c) replacement from amino acid 58 to 131; (d) insertion after amino acid 131; (e) refinement of the segment 58 to 133 (1000 steps); (f) refinement of segment 1–133 (100 steps).

MD as validation approach. Molecular dynamics simulation of crystallografic mP2 and I-FABP structures and the generated models were performed for modelling validation purposes. The GROMOS87 program package was used for calculations [29]. The four starting structures were energy minimized. First 1000 steps using the steepest descent algorithm were carried out and thereafter 1000 steps using the conjugate gradients algorithm. The minimized conformers were taken as input for the MD simulation. The D4 force field was employed [29, 30]. The time step for integration was 2 fs with bonds constrained according to the SHAKE algorithm [31]. Long range forces were calculated with the charge group technique and a clean cutoff of 12 Å. The molecular pair list was updated each 10th step for all non-bonded interactions below 8 Å. Coulomb interactions between 8 and 13 Å were updated every 20 fs. Temperature was kept constant at 293 K by coupling to Berendsen's thermal bath [32] with a relaxation parameter $\tau = 0.01$ ps during the full run. The system contain 1331 atoms including polar hydrogens. Initial velocities were assigned from a Maxwedellian distribution at 293 K. Rotational and translational motions were removed upon initialization.

The D4 parameter set represents conditions simulating a globally neutral protein. The polar side chains are assumed to be neutralized by counter ions and solvent polarization effects [30]. The only missing surrounding medium effect is the collision with actual water molecules. Thus the name of the model: non-inertial solvent (NIS). This model provides a fast and useful approach to sense atomic fluctuations around well defined X-ray structures. As early as 1985, this approach was proposed and tested in an MD study of the C-terminal fragment of the L7/L12 ribosomal protein, where collective secondary structure motion was found in a 150 ps trajectory [30]. This one was extended to 800 ps [33] producing, for the first time, stationary trajectories (i.e. the correlation functions calculated were independent of the time origin). Another example is the carboxy peptidase inhibitor protein from potatoes which has given excellent results with NIS simulations [34, 35]. The quality has been checked recently with simulations carried out in water [36]. With this MD approach, Åqvist et al. predicted the structure of the apo form of retinol binding protein [18, 37]. The holo form was known, but it was thought that the apo was not stable. The MD simulations, and later on X-ray crystallography, showed that the apoform was stable on its own. These and other results suggest that the MD techniques can be safely used to test the quality of a model built protein. An interesting feature of a NIS simulation is that biomolecules having structural defects usually develop unstable fluctuation patterns. The simulations are sufficiently reliable in this respect to be useful as validation criterion for a given static model.

Time series, energies, root mean square deviations (rms), temperature (B)-factors of all trajectories were analyzed with standard procedures and the mdFRODO [28] package .

The crystllographically seeded simulations display a relatively stationary trajectory beyond 200 ps. Myelin P2 drifts sligthly towards a lower energy structure as shown in Figure 2. This result is found for simulations where the solvent collisions are not included. Note that this statement corresponds to proteins simulated in the absence of water molecules which thereafter are compared with simulations in water [36, 38, 39]. A simulation carried out in the absence of discrete water molecules usually evolves in an implosive manner so that it maximizes the attractive interactions. On the contrary, it is believed that solvent collisions will affect the dynamics behavior, but not the average properties. This is actually found in simulations where water enters as discrete molecules [36] but the resources required to carry out the job

are too large to serve as a relatively rapid validation procedure.

For I-FABP, in the zone between 160 ps and 250 ps, there is a change in the total energy as a function of time (Figure 2). It presents a somewhat abrupt change. From there on, the trajectory looks pretty much stationary. However, as can be seen in Figure 3, there is no appreciable conformational change. This is not an unusual result for a multiparameter problem with large cross correlations. Small conformational changes may lead to noticeable changes of total energy but such structural changes are almost impossible to identify with the analytical techniques normally used.

The control simulations were considered then as representative of stable structures under the simulation conditions.

The modelled EgDf1 against myelin P2 and I-FABP display a clear stationary behavior from about 100 ps to 500 ps. It is thus reasonabler to assign a label of good structural quality to the modelled structures.

Results

Topology. The structure of EgDf1 modelled from mP2 is shown in Figure 1. EgDf1 has 133 residues: 11% are in α-helical conformation, 61% in β-sheet conformation and the rest in a loop conformation. Here, EgDf1 folds in a β-barrel topology formed by 10 antiparalel β-strands. The top sheet is formed by strands 1–5, and the bottom sheet by 7–10. Strand 6 is shared by the two sheets. Strands 1 and 2 are connected by a helix-turn helix motif, which closes one of the entrances of the barrel. The β-barrel structure shows the following topology: β1-L1.1-α1-L1.2-α2-L2.2-β2-L2.3- β3-L3.4-β4-L4.5-β5-L5.6-β6-L6.7-β7-L7.8-β8-L8.9-β9-L9.10-β10. (α = α-helix, β = β-strand, L=loop). Helix α1 spans over residues 16–22, α2 over 27–34 and strand β1 consists of residues 6–13, β2 of 39–45, β3 of 48–56, β4 of 59–65 , β5 of 70–75, β6 of 78–88 β7 of 91–98, β8 of 101–110, β9 of 113–120 and β10 of 123–131.

Fluctuation patterns. The Cα overlays display of the mP2, I-FABP, and of both models EgDf1(mP2) and EgDf1(I-FABP) are shown in Figures 3a–d. The pictures portray the idea of stable structural fluctuations except for one case.

Both X-ray and EgDf1 modelled from mP2 maintain the closed β-barrel structure along the entire trajectory of 500 ps. The overall fold and the secondary structural elements are well conserved. The largest deviations are produced in the loop regions, mainly in L3.4 and L5.6. For instance, L3.4 has an atom peak deviation of 3.6 Å and L5.6 of 3.8 Å (side chain) and of 3.4 Å and 3.0 Å for all atoms. The initial configuration is showed in red and the final reached region in yellow.

The MD simulation for EgDf1(I-FABP) is shown in Figure 3d. This trajectory evolves to a very different structure from the initial one, with big changes in the configuration of the α helices. The L5.6 loop migrates to a new configuration. Both movements cause an opening of the entrance in the protein. From these results it is apparent that the α2 helix and L5.6 are part of a deformable and possibly less stable region in the simulated EgDf1 molecule.

As noticed by a referee, there is a contrastthere with the energetics. As commented before, a relatively small step in the energy profile does not necessarily correlate with a visible conformational change. In fact, starting from the energy optimized X-ray coordinate, the simulation generates a large energy difference after 10 ps with an rms distance deviation below or around 2 Å. Thus, one way to be on the safe side, in so far as structural stability is concerned, is to run a trajectory in the range of 500 ps. In this case, the system may have a chance to find out different conformations generated by one or several instabilities built in to the modelling process.

Structural deviations. The rms differences (not shown) from the energy minimized initial conformations along the trajectories evidence that mP2, I-FABP and EgDf2(mP2) are stable at this level of simulation. The final all non-hydrogen atom coordinate rms differences are about 1.7 Å in the mP2 and EgDf1(mP2) models and 1.5 Å in the I-FABP. If only α-carbon are included in the calculation, the values become: 1.4 Å for the mP2 and EgDf1(mP2) and 1.2 Å for the I-FABP. The rms performance for the EgDf1(I-FABP) is completely different of other models. The final all non-hydrogen atom coordinate rms reaches a maximum value of 5.4 Å in 100 ps, and after this time fluctuates around a value of 5.0 Å away from the initial structure. This deviation corresponds with the big shift shown in Figure 3d for the α2 helix and L5.6. In view of the homology and identity scores of EgDf1 with mP2, the MD results concur to a choice of the EgDf1 (mP2) whose coordinates are used now to discuss other issues as if it were a true X-ray structure, for instance for docking studies.

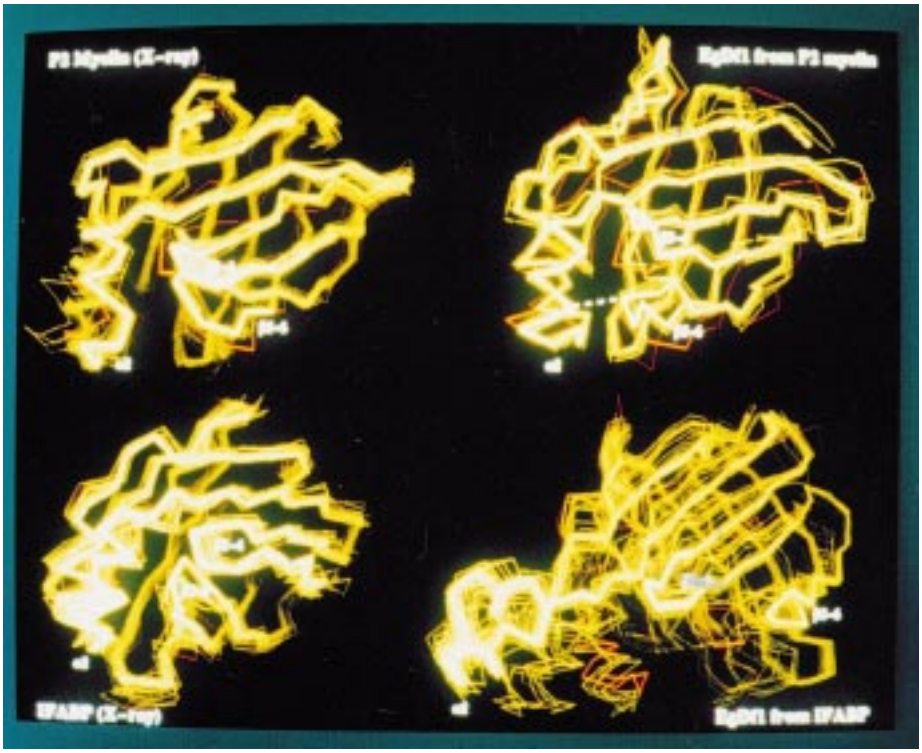

Figure 3. Superposition of backbone snapshots from the 500 ps trajectories shown in steps of 15 ps. mdFrodo program [28] was used as the graphic utility.

The rms deviations for each one of the secondary structural elements were analyzed for the EgDf1(mP2) model. The deviations for all atoms are between 0.7 and 1.6 Å for β-strand folding and between 0.8 and 2.0 Å for side chain atoms of β-strands. α-Helices rms deviations are between 1.1 and 1.6 Å for all atoms and between 0.14 and 0.2 for side chain atoms.

The rms deviations of the loops are between 0.6 and 2.0 Å for all atoms and between 0.8 and 2.8 Å for all side chain atoms. However, loops between β-3 and β-4 (L3.4) and between β5 and β6 (L5.6) presents high values of 3.4 and 3.0 Å (all atoms) and 3.4 and 3.8 Å (side chain atoms).

Atomic position fluctuations. Isotropic α-carbon and side-chain average B-factor for the EgDf1(mP2) structure are calculated from the trajectory and shown in Figure 4. Comparisons are made between the simulated crystal mP2 and model EgDf1. Some comparisons are made with crystallographic data in the figure caption. The values reported here may help the reader to sense zones having different fluctuation patterns. They should be used as qualitative sensors.

Leu 23, 27 and 32 in mP2 present high values. This is not the case for the analogous residues in EgDf1, even if they are conserved. However, they are residues with high B-temperature factor values in the EgDf1 model in this region (Arg 22, non conserved in mP2(Ala 22)). All these residues are in the α-helices region, previously detected as a quite deformable region .

Glu 98 in mP2 (Lys 99 in EgDf1), Asp 87 and Phe 57 show similar values in the side chain average behaviour in the mP2 as well as in the EgDf1 structures. Phe 57(58) belong to the L3-4 loop that is a deformable (plastic) zone.

EgDf1 show a higher value for Arg 76, a non conserved residue in mP2 (Ala 75). This residue is located in the L5-6 loop, with a temperature factor value of 110 A^2. In the mP2 structure this residue is an Ala(75) and its temperature factor is lower (33 A^2).

Higher values of temperature factors for mP2, coincident with high values for the EgDf1 model, are found in the region of L7.8(Asp 98, Lys 99 in EgDf1).

Molecular complexes. Taking as a template the X-ray complex structures and position of palmitic acid

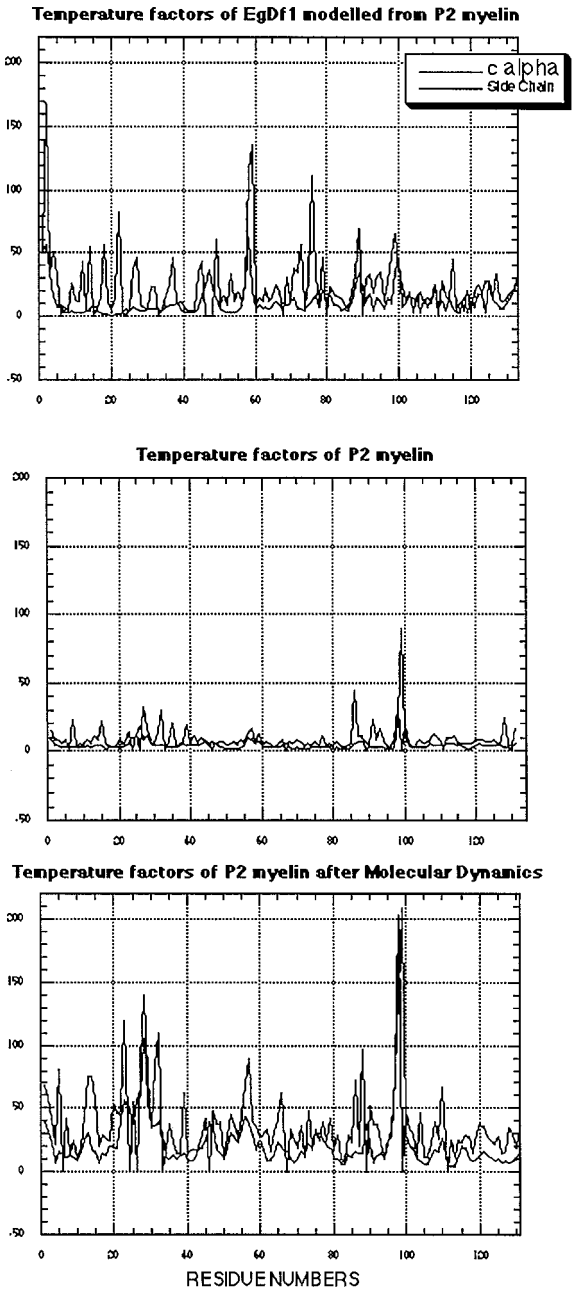

Figure 4. Isotropic α-carbon and side-chain average B-factors (Å^2). From top to bottom: EgDf1(mP2); X-ray data for P2 myelin; simulated data for P2 myelin. The B-factors for simulated P2 myelin are larger than the crystal ones. This is largely due to the absence of explicit water molecules in the simulations. Otherwise, trends are fairly satisfactory. For instance, around residue 99 both the X-ray and MD simulation show large relative fluctuations.

(PA) in I-FABP-PA and of oleic acid (OA) in mP2-OA, we modelled two putative ligands inside the structure of EgDf1(mP2).

The amino acid residues contacting at less of 3.7 Å were analyzed for all X-ray and modelled structures; the invariant side chains of the latter correspond to the X-ray structure rotamers. The results are presented in Table 1 and shown in Figure 1. The carboxylates of both ligands make contacts with Arg 107, Arg 127 and Tyr 129. The fatty acid hydrocarbon chain is buried into a cavity mostly constituted by hydrophobic residues (81% of contacting residues). Side chain movements were necessary to make room for the polar head and hydrophobic tail of both ligands. It was possible to accomodate completely the bent chain of oleic acid, having enough room inside our model. This was not the case for the selected elongated conformation of palmitic acid. The chain end protruded through the barrel entrance and colapsed over some residues of this region.

There exists the possibility of a secondary binding site for the fatty acid as has been recently shown for the crystal structure of a recombinant form of rat liver fatty acid-binding protein by Thomson et al. [40]. Such a possibility will be explored in future modelling work.

Discussion

The structural and MD results will be discussed now with special reference to three topics: putative major epitopic regions, consensus phosphorylation motifs and substrate characteristics. Major antigenic determinants of EgDf1 and phosphorylation motifs were previously suggested from sequence analysis [1, 2]. The EgDf1 modelled from myelin P2 was used to visualize the orientation and accesibility to the solvent of side chains in the detected regions.

Putative major epitopic regions. Three highly hydrophilic regions detected (EP1, EP2 and EP3 in the Figure 4) were previously localized at positions 95–101 (Glu-Gln-Asp-Asp-Lys-Thr-Lys), 9–14 (Lys-Met-Glu-Lys-Ser-Glu) and 68–73 (Gly-Glu-Lys-Lys-Phe-Lys-Glu). EP1 belongs mainly to the β7 strand and loop L7.8 [1]. The methods used by Esteves et al. were those reported by Hoop and Woods [41], Karplus and Schulz [42] and Nishikawa and Ooi [43]. According to the model structure, EgDf1 has 71% of its residues exposed to the solvent and side chains of

Table 1. The amino acid residues contacting at less than 3.7 Å were analyzed for all X-ray and modelled structures. All residues making contact with any of the molecules are presented The number of scores being larger for oleic acid, this one is suggested to be the best ligand

	IFABP palmitic	EgDf1 palmitic	EgDf1 oleic	MP2 oleic
F16	**Y**	*	*	*
I19				**Y**
M20		*	*	*
V25			*	
T29		*	*	*
G33		*	*	*
P38			*	
I40			*	
F58		*		
F65	*			
R76			*	D
F77		*	*	
R79		*	*	
V87	W			
I104				*
R107	*	*	*	*
A115	Q			V
R127		*	*	*
Y129		*	*	*

Gln 96 and Asp 98 towards the centre of the barrel. The region EP2 starts at the end of β1 and expands at the L1.2 with its last residue. It has 83% solvent oriented amino acid residues. The region EP3 is located at the end of the loop L4.5 and includes almost all of the β5 strand. In the model this region is completely exposed to the solvent, an interaction with an antigen is therefore possible.

Antigen-antibody interactions may be modulated by the rigidity/flexibility ratio of the epitope. For this reason, it is interesting to examine rms and temperature factors of β1 and Lβ1-α2 for EP2, L4.5 and β5, β7 for EP3 and L7.8 for EP1. The rms deviation for Lβ1-α2 has a maximum value of 2.8 Å (side-chains), and temperature factors denoting zones of small amplitude fluctuation. Similar results are observed for L4.5 in Ep3 with an rms of less than 0.2 (side chain) and a temperature factor less than 50 A^2. Finally, β7 and L7.8 show the lowest values of rms. However, there is a value of 70 A^2 for Lys 99 in L7.8 of EP1.

If we take into account both the hydrophilic pattern and the mobility properties of these three putative regions, we could suggest the EP1 region as having the highest probability to be an epitope.

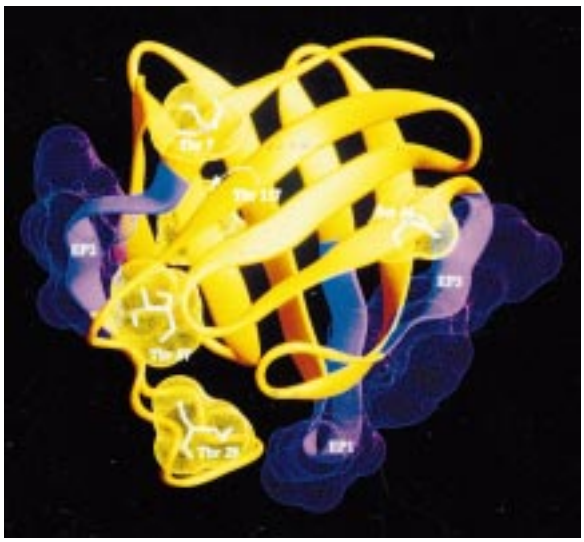

Figure 5. EgDf1 modelled from mP2: epitopic predicted regions are depicted in magenta. Phosforylation motifs are shown as white sticks.

Consensus phosphorylation motifs. Protein kinase C and related signalling pathways recognize the consensus sequences [Ser/Thr]-x-[Lys/Arg] [44]. Amino acids Thr 7, Thr 29, Thr 57, Ser 64, Thr 117 that could serve as phosphorylation targets for protein kinase C and are located in the following regions of the protein: Glu-Ala-Phe-Leu-Gly-**Thr**-Trp-Lys-Met-Glu-Lys; Gly-Val-Asp-Val-**Thr**-Arg-Lys-Asn-Gly-Asn; Met-Arg-Ser-Glu-ser- **Thr**-Phe-Lys-Thr-Glu-Glu; Lys-Thr-Thr-Glu-Cys-**Ser**-Phe-Lys-Leu-Gly-Glu; Met-Glu-Leu-Lys-Ala-**Thr**-Val-Lys-Asp-Glu. Threonine 7 belongs to the β1, Thr 29 to the α2, Thr 57 to the L3.4, Ser 64 to the β4 and Thr 117 to the β9 secondary elements. All of them would be exposed to the solvent if the model structure is correct and, consequently, they may easily be attacked.

Significance. The model 3D structure allows for a clear display of putative epitopic zones and phosphorylation sites in EgDf1. All of them were suggested by comparisons using the sequence only [41]. The results herein obtained indicate that all these regions are solvent accessible, and, consequently, they may well be operating in vivo. Of course, the presence of an accessible phosphorylating site must be experimentally tested. If the molecule were actually to be phospho-

rylated, one way to map out the sites is given by site directed mutagenesis techniques.

Taking into account that homologous proteins in *Fasciola hepatica* and *Schistosoma mansoni* have shown to have immunoprotective activity in animals with experimental infection, the evaluation of putative epitopes in the EgDf1 protein may be an important contribution to initiate immunological studies.

The knowledge of lipids and lipid metabolisms in *Echinococcus* is limited [45–46]. However, it is known that the major fatty acids of cestodes are usually C16 and C18, with the oleic acid (C 18:2) being the major C18 acid, albeit linoleic (18:2) and stearic (18:0) predominate in some species. Platyhelmints are unable to synthesize de novo their own lipids but they can elongate the fatty acids taken from the host. The fact that oleic acid seems to be an adequate ligand for EgDf1 could be correlated with the abundance of this fatty acid in platyhelmints. EgDf1 may be involved in the process of supplying fatty acids for membrane biosynthesis and signaling pathways. In summary, the molecular modelling techniques used here predict oleic acid as a possible ligand for EgDf1 (cf. Figure 1). Again, experiment will say the last word.

Acknowledgements

The authors thank SAREC and UNDP-project (URU/84/002-PEDECIBA) for financial support. O.T. acknowledges financial support from NFR (Sweden).

References

1. Esteves, A., Dallagiovanna, B. and Ehrlich, R., Mol. Biochem. Parasitol., 58 (1993) 215.
2. Esteves, A., Joseph, L., Paulino, M. and Ehrlich, R., Int. J. Parasitol., 27 (1997) 1013.
3. Scapin, G., Gordon, J.I. and Sacchettini, J.C., J. Biol. Chem., 367 (1992) 4253.
4. Mueller-Fahrnow, A., Egner, U., Jones, T.A., Ruedel, H., Spener, F. and Saenger, W., Eur. J. Biochem., 199 (1991) 271.
5. Xu, Z., Bernlohr, D.A. and Banaszak, L.J., J. Biol. Chem., 268 (1993) 7874.
6. Xu, Z., Bernlohr, D.A. and Banaszak, L.J., Biochemistry, 31 (1992) 3484.
7. Bohmer, F.D., Kraft, R., Otto, A., Wernstedt, C., Hellman, U., Kurtz, A., Moller, T., Rohde, K., Etzold, G., Lehmann, W., Langen, P., Heldin, C.-H. and Grosse, R.J., Biol. Chem., 262 (1987) 15137.
8. Spener, F., Unterberg, C., Borhcers, T. and Grosse, R., Mol. Cell. Biochem., 98 (1990) 57.
9. Maatman, R.G.H.J., Degano, M., Van Moerkerk, H. T.B., Marrewijk, W.J.A., Van Der Horst, D.J., Sacchettini, J.C. and Veerkamp, J.H. Eur. J., Biochem., 221 (1994) 801.
10. Benning, M.M., Smith, A.F., Wells, M.A. and Holden, H.M., J. Mol. Biol., 228 (1992) 208.
11. Tapia, O. and Åqvist, J., Prog. Clin. Biol. Res., 289 (1989) 55.
12. Rein, R. and Golombek, A. (Eds.) Computer-assisted Modeling of Receptor-Ligand Interactions, Alan R. Liss, New York, NY, 1989.
13. Bamborough, P. and Cohen F.E., Curr. Opin. Struct. Biol. 6 (1996) 236.
14. Bajorath, J. and Aruffo, A., J. Comput.-Aided Mol. Design., 9 (1997) 319.
15. Jones, T.A., Cowan, S.W., Newcomer, M.E. and Bergfors, T., Frontiers in Drug Research, Alfred Benzon Symposium, 28 (1990) 267.
16. Newcomer, M.E., Jones, T.A., Åqvist, J., Sundelin, J., Eriksson, U., Rask, L. and Peterson, P. A., EMBO J., 3 (1984) 1451.
17. Jones, T.A., Bergfors, T., Sedzik, J. and Unge, T., EMBO J., 7 (1988) 1597.
18. Åqvist, J., Sandbolm, P., Jones, T.A., Newcomer, M.E., van Gunsteren, W.F. and Tapia, O., J. Mol. Biol., 192 (1986) 593.
19. Åqvist, J., J. Mol. Struct. (THEOCHEM), 256 (1992) 135.
20. Monaco, H.L., Rizzi, M. and Coda, A., Nature, 268 (1995) 1039.
21. Richards, W.G. (Ed.) Computer-aided Molecular Design, IBC Technical Services Ltd., London, 1989.
22. Kollman, P.A. and Merz, J.M., Acc. Chem. Res., 23 (1990) 246.
23. Tapia, O., Oliva, B., Nilsson, O., Querol, E. and Avilés, F.X., In Giralt, E. and Andreu, D. (Eds.), ESCOM, Leiden, 1991, pp. 581–XXX.
24. Bertran, J. (Ed.) Molecular Aspects of Biotechnology: Computational Models and Theories, Kluwer Academic Publishers, Amsterdam, 1992.
25. Horjales, E., Oliva, B., Stamato, F.M.L.G., Paulino-Blumenfeld, M., Nilsson, O. and Tapia, O., Mol. Eng., 1 (1992) 357.
26. Karplus, M. and Petsko, G.A., Nature, 347 (1990) 631.
27. Cambillau, C.C. and Horjales, E., J. Mol. Graph., 5 (1987) 174.
28. Nilsson, O., J. Mol. Graph., 8 (1990) 192.
29. van Gunsteren, W.F. and Berendsen, H.J.C., Groningen Molecular Simulation (GROMOS) Library Manual, BIOMOS B.V., Groningen, 1987.
30. Åqvist, J., van Gunsteren, W.F., Leijonmarck, M. and Tapia, O., J. Mol. Biol., 83 (1985) 461.
31. Ryckaert, J.-P., Ciccotti, G. and Berendsen, H.J.C., J. Comput. Phys., 23 (1977) 327.
32. Berendsen, H.J.C., Postma, J.P.M., van Gunsteren, W.F., DiNola, A. and Haak, J.R., J. Chem. Phys., 81 (1984) 3684.
33. Tapia, O., Nilsson, O., Campillo, M., Åqvist, J. and Horjales, E., In Sarma, R.H. and Sarma, M.H. (Eds.), DNA Protein Complexes and Proteins, Vol. 2, Academic Press, New York, NY, 1990, p. 147.
34. Oliva, B., Wästlund, M., Nilsson, O., Cardenas, R., Querol, E., Avilés, F.X. and Tapia, O., Biochem. Biophys. Res. Commun., 176 (1991) 616.
35. Oliva, B., Nilsson, O., Wästlund, M., Cardenas, R., Querol, E., Avilés, F.X. and Tapia, O., Biochem. Biophys. Res. Commun., 176 (1991) 627.
36. Daura, X., Oliva, B., Querol, E., Avilés, F.X. and Tapia, O., Proteins, 25 (1996) 89.
37. Sandblom, P., Åqvist, J., Jones, T.A., Newcomer, M.E., van Gunsteren, W.F. and Tapia, O., Biochem. Biophys. Res. Commun., 139 (1986) 564.

38. Åqvist, J., Leijonmarck, M. and Tapia, O., Eur. Biophys. J., 16 (1989) 327.
39. Åqvist, J. and Tapia, O., Biopolymers, 30 (1990) 205.
40. Thomson, J., Winter, N., Terwey, D., Bratt, J. and Banaszak, L., J. Biol. Chem., 272 (1997) 7140.
41. Hoop, T.P. and Woods, K.R., Proc. Natl. Acad. Sci. USA, 78 (1981) 3824.
42. Karplus, P.A. and Schulz, G.E., Naturwissenschaften, 72 (1985) 212.
43. Nishikawa, K. and Ooi, T., J. Biochem. (Tokyo), 100 (1986) 1043.
44. Kishimoto, A., Nishiyama, K., Nakanishi, G., Uratruji, Y., Namura, H., Takamaya, Y. and Nishizuka, J., J. Biol. Chem., 260 (1981) 12492.
45. McManus, D.P. and Bryant, C., In Thompson, R.C.A. (Ed.), The Biology of Echinococcus and Hydatid Disease, George Allen & Unwin, London, 1986, p. 127.
46. Smyth, J.D. and McManus, D.P., The Physiology and Biochemstry of Cestodes, Cambridge University Press, Cambridge, 1989.
47. Carson, M., J. Mol. Graph., 5 (1987) 103.